Article

Buffer Effects in Zirconium-Based UiO Metal−Organic Frameworks (MOFs) That Influence Enzyme Immobilization and Catalytic Activity in Enzyme/MOF Biocatalysts

Raneem Ahmad, Sydnie Rizaldo, Mahnaz Gohari, Jordan Shanahan, Sarah E. Shaner, Kari L. Stone,* and Daniel S. Kissel*

Read Online

ACCESS | Metrics & More | Article Recommendations

ABSTRACT: Novel biocatalysts that feature enzymes immobilized onto solid supports have recently become a major research focus in an effort to create more sustainable and greener chemistries in catalysis. Many of these novel biocatalyst systems feature enzymes immobilized onto metal−organic frameworks (MOFs), which have been shown to increase enzyme activity, stability, and recyclability in industrial processes. While the strategies used for immobilizing enzymes onto MOFs can vary, the conditions always require a buffer to maintain the functionality of the enzymes during immobilization. This report brings attention to critical buffer effects important to consider when developing enzyme/MOF biocatalysts, specifically for buffering systems containing phosphate ions. A comparative analysis of different enzyme/ MOF biocatalysts featuring horseradish peroxidase and/or glucose oxidase immobilized onto the MOFs UiO-66, UiO-66-NH$_2$, and UiO-67 using a noncoordinate buffering system (MOPSO buffer) and a phosphate buffering system (PBS) show that phosphate ions can have an inhibitory effect. Previous studies utilizing phosphate buffers for enzyme immobilization onto MOFs have shown Fourier transform infrared (FT-IR) spectra that have been assigned stretching frequencies associated with enzymes after immobilization. Analyses and characterizations using zeta potential measurements, scanning electron microscopy, Brunauer−Emmett−Teller surface area, powder X-ray diffraction, Energy Dispersive X-ray Spectroscopy, and FT-IR show concerning differences in enzyme loading and activity based on the buffering system used during immobilization.
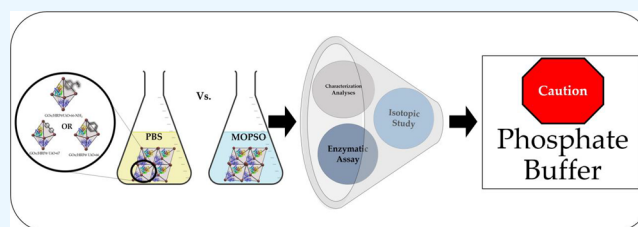
1. INTRODUCTION

One pivotal advancement in the development of sustainable chemical processes is the immobilization of enzymes onto solid supports to perform biocatalysis. Biocatalysts are often used as a more efficient and greener alternative to catalysis in industrial chemical processes[1−3] because of their ability to perform reactions under mild conditions with varied functionalities.[4] Biocatalysts that feature immobilized enzymes have shown improved catalytic activity, stability, recyclability, and functionality under extreme conditions.[5,6] Immobilization is the attachment of enzymes onto solid supports, which can be done using a variety of techniques. These techniques include physical adsorption, cross-linking, encapsulation, and chemical adsorption,[3,6] which can improve an enzyme's catalytic activity by preventing aggregation, promoting rigidification, and inhibiting contact with hydrophobic interfaces, such as gas bubbles.[7] Various solid supports have been reported as efficient substrates for enzyme immobilizations that have successfully improved enzyme functionalities.[8−16]

An additional benefit to immobilizing enzymes on solid supports is the ability to design biocatalytic systems that feature multiple, co-immobilized enzymes that can participate in cascade reactions.[1,2,15,17−20] Previously reported co-immobilized biocatalytic systems have been shown to perform reactions better due to the proximity between both enzymes on the solid support.[1,13,15,21−25] In this report, the enzymes glucose oxidase (GO$_x$) and horseradish peroxidase (HRP) were used to create a co-immobilized enzyme/metal−organic framework (MOF) biocatalytic system. GO$_x$ from *Aspergillus niger* (*A. niger*) is commercially available and utilized for its ability to produce hydrogen peroxide via oxidation of glucose.[26] HRP, in turn, catalyzes the oxidation of many organic substrates in the presence of hydrogen peroxide.[27] The two enzymes have been co-immobilized in previous studies for biotechnological applications, such as biosensing, using various solid support materials.[23,28−31]

This report focuses specifically on using MOFs as solid supports for enzyme immobilization. MOFs are coordination networks containing potential void spaces that feature inorganic nodes connected through organic linkers.[32] They are known for their porous properties and tunability, making them ideal for guest−host interactions.[3,33] MOFs have traditionally been used for a variety of applications including gas storage, sensing, and drug delivery, among others, but have recently become popular for enzyme immobilizations.[23,34] Many recent studies have reported successful enzyme immobilizations using MOFs to create composite materials for application in biosensing, proteomic analysis, synthesis, and water remediation.[35−40] These studies have used a variety of immobilization techniques including adsorption, encapsulation, and covalent bonding.[41−44] All of these immobilization techniques require a buffered system to maintain the functionality of the enzymes used during immobilization.

This study utilizes the zirconium-based MOFs UiO-67, UiO-66, and UiO-66-NH$_2$ to investigate enzyme immobilizations with HRP and/or GO$_x$ under different conditions. The UiO-66 and UiO-66-NH$_2$ MOFs are similar in pore size and structure, but UiO-66-NH$_2$ features an amine group off the 1,4-benzene-dicarboxylate linker, which has been shown to strengthen interactions at the enzyme/MOF interface thereby influencing enzyme adsorption.[22] The UiO-67 MOF is similar to UiO-66 but features an additional aromatic ring in its 4,4′-biphenyl-dicarboxylate linker that creates larger voids and slightly decreases framework stability.[45] Initially, the authors in this study attempted to create biocatalysts using these MOFs in a buffer containing phosphate ions to facilitate enzyme immobilizations via adsorption because of its accessibility and diverse pH ranges; however, the immobilized products showed little to no catalytic activity compared with the free enzyme in solution. These peculiar results prompted the authors to further investigate the conditions utilized during enzyme immobilization and their influence on the enzyme/MOF interface.

Fourier transform infrared (FT-IR) characterization of the enzyme/MOF products immobilized in phosphate buffer all showed a strong absorption around 1000 cm^{-1} that was initially attributed to an immobilized enzyme. This assignment was supported by other studies from the literature of similar enzyme/MOF systems created using phosphate buffer to facilitate immobilization. Several recent studies, such as that from Cao et al., have characterized this peak at 1000 cm^{-1} as the immobilized enzyme in the enzyme/MOF composite system.[37,38,46−48] The study from Cao et al. used FT-IR data of enzyme-immobilized UiO-66-NH$_2$ and a typical amide I fitting procedure to ascribe the secondary structure confirming the enzyme's presence and stability.[46] This peak is also present in several other enzyme immobilization studies that utilize UiO MOFs, as well as other MOFs from the MIL series, as solid supports.[14,37,47,49,50] The authors herein attest that this peak is attributable to phosphate ions and not to the attached enzyme.

Interestingly, the FT-IR peaks previously reported to confirm enzyme immobilization were not observed in FT-IR spectra taken of the enzyme/MOF composites after replacing phosphate buffer with MOPSO buffer during immobilization. This led to speculation as to whether the stretching frequency previously observed at 1000 cm^{-1} was truly the result of the immobilized enzyme or potentially from phosphate ions adsorbed in the enzyme/MOF composite systems. MOPSO buffer was used in this study for comparison with phosphate

buffer because of its ability to remain noncoordinate in solution and operate at a similar pH range.[51] FT-IR and isotopic study data collected during this investigation definitely show that the absorption peak at 1000 cm^{-1} previously thought to confirm enzyme immobilization actually arises from phosphate ions trapped in the pores of the MOF substrate. Additionally, an investigation into the catalytic activity of enzyme/MOF composites immobilized in both phosphate and MOPSO buffers shows that adsorbed phosphate ions actually inhibit enzyme loading, which limits catalysis.

2. EXPERIMENTAL SECTION

2.1. Materials. Zirconium(IV) chloride, purchased from ACROS Chemistry (AR purity 97%), terephthalic acid and 2-aminoterephthalic acid purchased from Sigma Aldrich (AR purity <99%) were used as precursors for UiO-66 and UiO-66-NH$_2$. N,N-dimethylformamide (DMF), purchased from Fisher Scientific (AR purity <99%), was used as a complexing solvent. 2-Hydroxy-3-morpholinopropanesulfonic acid (MOPSO) was purchased from Sigma Aldrich. All chemicals are analytical grade and were used without any further purification. HRP (~150 U/mg) and GO$_x$ from *A. niger* (50,000 U) were purchased from Tokyo Chemical Industry (TCI) and Sigma Aldrich.

2.2. MOF Synthesis. The synthesis of UiO-67 was performed as a one-pot synthesis in a Baoshishan hydrothermal synthesis autoclave reactor with a Teflon-lined reaction vessel based on a solvothermal technique modified from Shearer et al. using biphenyl-4,4′-dicarboxylic acid (bpdc) in place of 1,4-benzendicarboxylic acid (bdc).[33] Zirconium(IV) chloride (1.98 mmol) and bpdc (1.98 mmol) precursors were dissolved in 40 mL DMF in the reaction vessel. An addition of 342 μL of concentrated hydrochloric acid moderator was then added to improve ligand solvent exchange. The solution was heated at 120 °C in a stainless steel solvothermal reactor for 24 h. The resulting MOF precipitate was collected and washed three times with DMF, then left to soak in methanol for 24 h to activate the pores. After soaking for 24 h, the UiO-67 product was collected by vacuum filtration and washed three times with methanol, then heated in an oven at 110 °C overnight. This process was repeated for the synthesis of UiO-66 and UiO-66-NH$_2$ substituting the appropriate bdc linker for bpdc. Functional groups of the MOF composites were identified using Fourier transform infrared attenuated total reflectance (FT-IR-ATR) spectroscopy on a CARY 630 FT-IR spectrometer.

2.3. Enzyme Immobilization. Enzymes were immobilized by suspending 50 mg of MOF into a centrifuge tube containing 450 μL of buffer, 25 μL of GO$_x$ (5 mg/mL), and 25 μL HRP (5 mg/mL). After 24 h of incubation, the enzyme/MOF composites were filtered, washed with ethanol, and dried. The following enzymes used in this study were purchased in the solid state: GO$_x$ from *A. niger* 145,200 U/g from Sigma Aldrich, and horse radish peroxidase 190 U/mL from TCI. The 50 mM phosphate buffer was prepared by diluting 1 M stock of phosphate buffer that was prepared from 85.3% phosphoric acid and pH adjusted with 6 M NaOH. The 50 mM MOPSO buffer was prepared by diluting Bioworld 0.2 M MOPSO buffer with a pH of 6.5, and the pH was adjusted using 6 M NaOH.

2.4. Enzymatic Assay. The colorimetric purpurogallin enzyme assay mixture consisted of the following glucose to pyrogallol ratio in millimoles: 56:127 and 10 mg of enzyme/
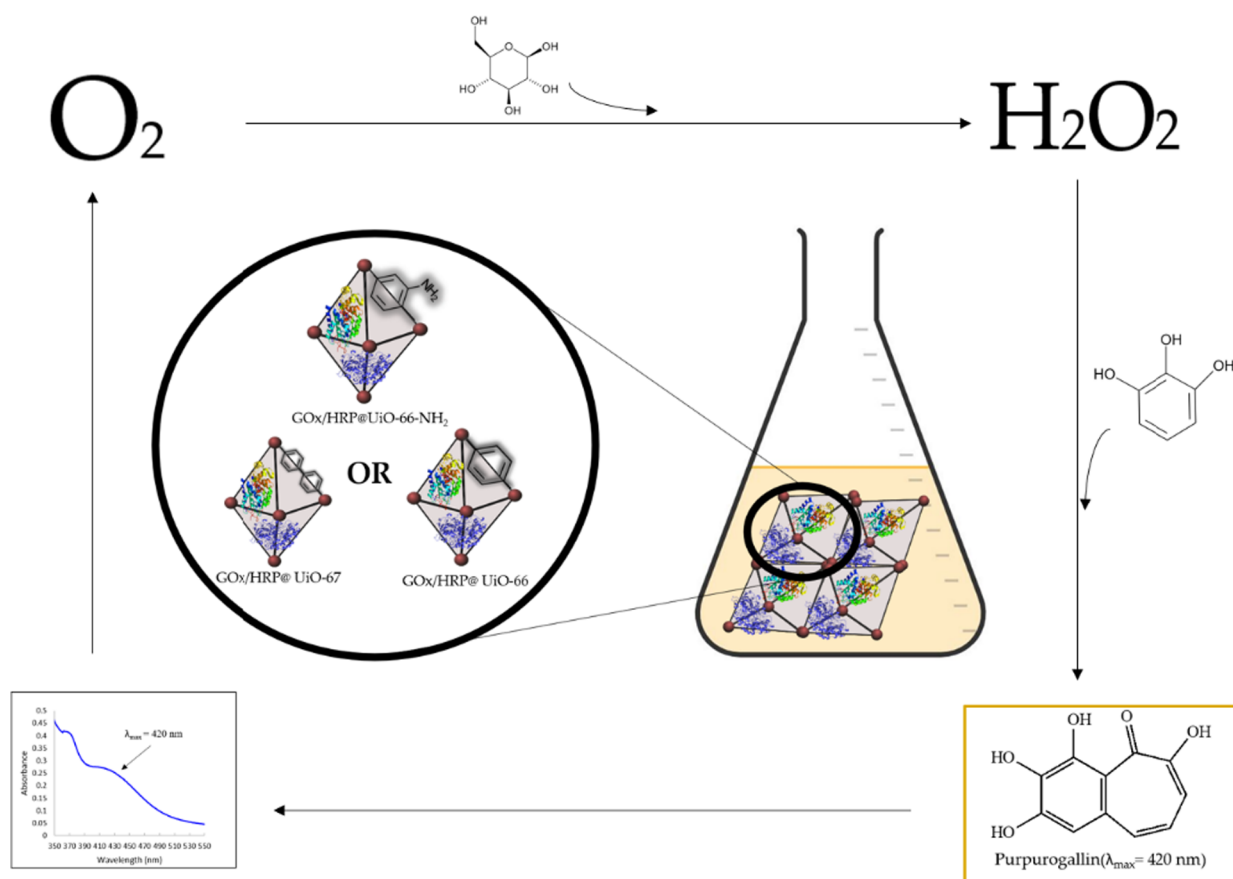
Figure 1. Pyrogallol enzymatic assay. The reaction scheme for the pyrogallol enzymatic assay to test the catalytic activity of the three enzyme/MOF composites.

MOF composite. After running the reaction for 3 min, the enzyme/MOF composite was filtered, and the absorbance of the reaction solution was taken using a Vernier SpectroVis Plus Spectrophotometer to calculate concentration of synthesized purpurogallin.

2.5. Isotopic Study. The isotopic study was performed by preparing phosphate-labeled buffer from potassium dihydrogen phosphate ($^{18}O_4$, 95%) purchased from Cambridge Isotopic Laboratories, Inc. The pH was adjusted to 7.00 using 2.0 M KOH. Each enzyme solution (GO_x and HRP) was then prepared using the isotopic buffer to a concentration of 5 mg/mL. The UiO-67 MOF was soaked overnight in 450 μL of buffer, and 25 μL of each isotopically labeled enzyme solution containing GO_x or HRP. Isotopically labeled composites were washed with ethanol and dried in a desiccator before characterization.

2.6. Instrumentation. Functional groups of the pure and isotopically labeled enzyme/MOF composites were identified using FT-IR-ATR spectroscopy on a CARY 630 FT-IR spectrometer. Powder X-ray diffraction (PXRD) data of the MOF and enzyme/MOF composites were collected on a Rigaku SmartLab SE diffractometer using a copper anode with $K\alpha_1 = 1.54056$ Å and $K\alpha_2 = 1.54439$ Å fitted with a nickel $K\beta$ filter. Samples were analyzed between 2θ 5 and 80° with a step size of 0.01 degrees and a scan speed of 1 degrees/min. Zeta potentials of the pure and enzyme/MOF composites were obtained using a Malvern Zetasizer Nano ZS. Each solution was prepared by dissolving 2 mg of MOF, 10 μL of HRP, and 10 μL of GO_x into 15 mL of 50 mM PBS with a pH of 7.00.

Nitrogen adsorption isotherms were obtained at 77 K using a Quantachrome NOVAtouch LX[4] Surface Area and Pore Size Analyzer. Samples were prepared by soaking UiO-66, UiO-66-NH_2, UiO-67, HRP/GO_x@UiO-66, HRP/GO_x@UiO-66-NH_2, and HRP/GO_x@UiO-67 in either MOPSO or PB for approximately 24 h before degassing at 25 °C for 24 h. Surface area measurements were determined using the Brunauer−Emmett−Teller (BET) method, and total pore volume and average pore size measurements were also obtained. Scanning electron microscopy (SEM) with complimentary energy dispersive X-ray spectroscopy (EDS) measurements were collected on a JEOL JCM-7000 SEM using a secondary electron detector. All samples were precoated using 5 nm Au nanoparticles to reduce charging.

3. RESULTS AND DISCUSSION

3.1. Enzyme Activity. The effects of the two different buffers on activity of the enzyme/MOF composites were determined by studying the catalytic oxidation of pyrogallol to purpurogallin. This colorimetric assay measures the enzymatic activity and tests the bienzymatic system of HRP and GO_x. Purpurogallin is synthesized from the oxidation of pyrogallol by HRP that is activated by peroxide produced from the oxidation of glucose in the presence of O_2 as shown in Figure 1.[52,53] The synthesis of purpurogallin can be monitored using UV−vis spectroscopy by observing increases in absorption at the λ_{max} of 420 nm. The experimentally determined activities of the free enzyme and enzyme/MOF composites in Table 1 show composites immobilized in MOPSO buffer performing

markedly better than composites immobilized in phosphate buffer.

Table 1. Comparison of Enzyme Activities from Biocatalysts Created Using PBS and MOPSO Buffers During Immobilization

	MOPSO activity (U/mg)[a]	PBS activity (U/mg)[a]
UiO-66	0	0
UiO-66-NH$_2$	0	0
UiO-67	0	0
GO$_x$/HRP@UiO-66-NH$_2$	198.36	42.31
GO$_x$/HRP@UiO-66	189.75	3.2933
GO$_x$/HRP@UiO-67	71.95	18.24
free HRP and GO$_x$	62.77[b]	50.69[b]

[a]Enzyme activity calculated from absorbance data of purpurogallin synthesis and normalized to the calculated enzyme loading onto GO$_x$/HRP@UiO-66-NH$_2$ in MOPSO in activity units (U per mg of enzymes) loaded onto composite. [b]Free enzyme activity calculated from absorbance data of purpurogallin synthesis in activity units (U per mg of enzymes).

The composite GO$_x$/HRP@UiO-66-NH$_2$ immobilized in MOPSO buffer showed the greatest enzymatic activity (198.36

U/mg), which is no surprise considering the amine-functionalized linker has been shown to enhance electrostatic interactions at the enzyme/MOF interface resulting in greater loading and activity.[22] Interestingly, the same composite system showed much lower activity (42.31 U/mg) when the enzyme immobilization was performed in phosphate buffer (PBS). This large discrepancy in enzyme activity was also observed in the bienzymatic composite systems for UiO-66 and UiO-67, which performed much better after immobilization in MOPSO buffer. Composites immobilized in phosphate buffer overall showed a maximum 98% decrease in activity compared to composites immobilized in MOPSO buffer as given in Table 1. The free enzyme solutions also showed greater catalytic activity in MOPSO compared with PBS, however, this discrepancy was not nearly as pronounced as those observed for the enzyme/MOF composites. These results strongly support the notion that the absorption peak observed at ~1000 cm^{-1} in the FT-IR spectra of the enzyme/MOF composite products is actually the result of adsorbed phosphate ions rather than confirmation of enzyme immobilization. This strong absorption peak was not observed in the FT-IR spectra of enzyme/MOF composite products immobilized in MOPSO, indicating that phosphate ions from PBS are adsorbing into the MOF pores during immobilization and acting as a potential barrier that inhibits enzyme loading. This
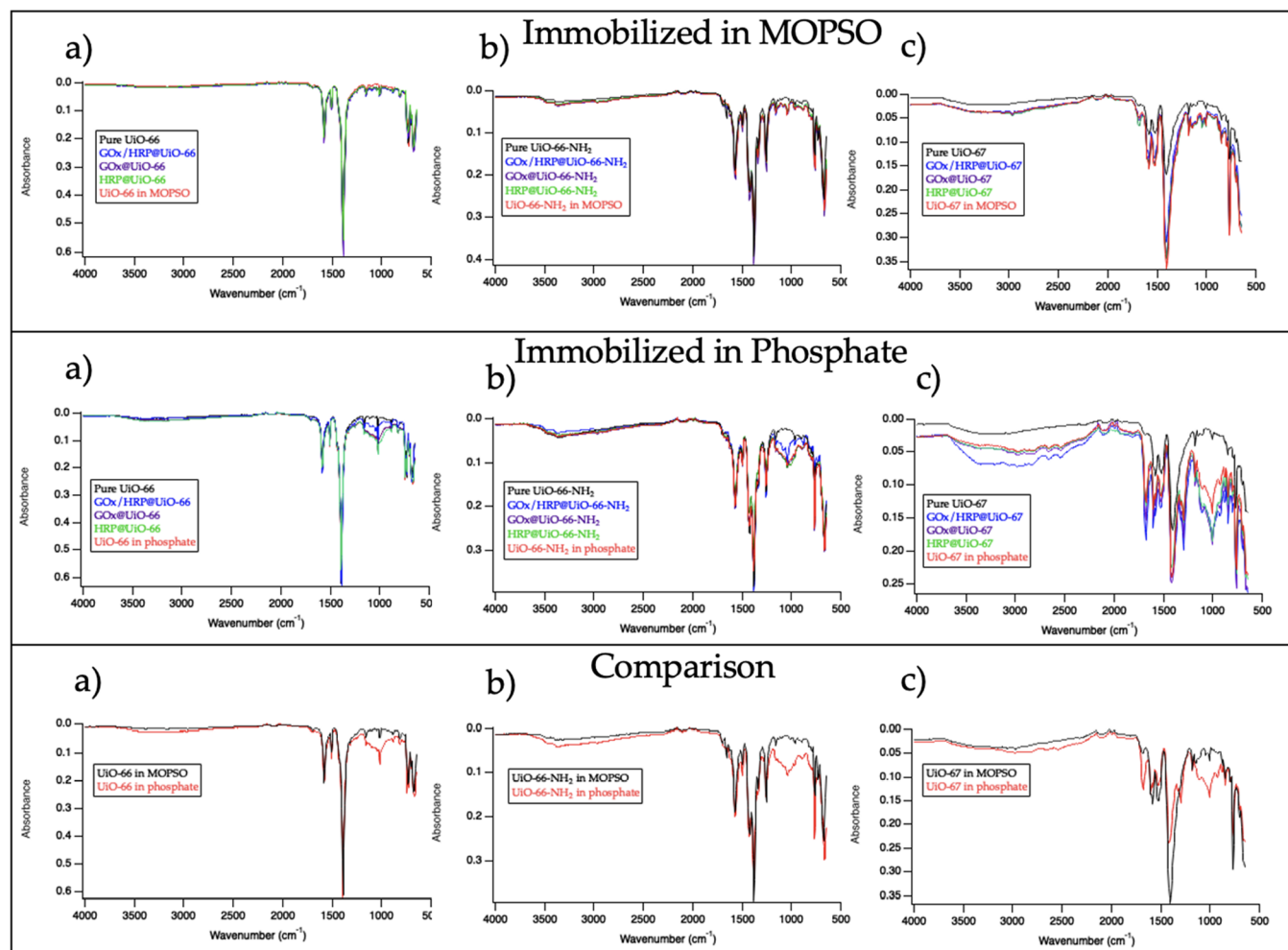

Figure 2. FT-IR spectra of MOF composites immobilized in MOPSO and phosphate buffers. Immobilized composites (a) UiO-66, (b) UiO-66-NH$_2$, (c) UiO-67 in MOPSO (top) and in PBS (bottom). Bottom panel shows comparison between MOPSO- and PB-soaked MOFs.

outcome of impairment in phosphate-buffered enzyme/MOF systems has also been reported in studies that utilize ZIF-8 and MIL-100 as solid supports, and even for other composite biocatalyst systems, such as lipase immobilized onto octyl-agarose.[48,54−57]

3.2. FT-IR Characterization.
The FT-IR spectra of all enzyme/MOF composites were taken after enzyme immobilization using both MOPSO and PBSs. In addition, all three MOFs were soaked in both buffers alone to mimic enzyme immobilization conditions and determine if the buffering systems were affecting the MOF substrates. The spectra for each MOF are shown overlayed with MOF after soaking in buffer alone, singly immobilized enzyme/MOF composites (with HRP or GO_x), and doubly immobilized enzyme/MOF composites (with both HRP and GO_x) for each buffer system in Figure 2.

The spectrum of the synthesized UiO-67 powder (Figure 2c) shows COO^- symmetric and asymmetric stretching at 1565 and 1408 cm^{-1} characteristic of bridging coordination from the carboxylate linker to the Zr nodes reported for UiO-67.[58] Additional peaks appearing at 1558 and 1207 cm^{-1} arise from the C−C ring stretching and C−H bending in the ring. These strong absorption peaks are retained in the spectra of UiO-67 after exposure to PBS (Figure 2c) indicating the carboxylate coordination is retained in the PBS-soaked MOF; however, there is a considerable hypsochromic shifting of minor MOF peaks observed from 900 to 1200 cm^{-1}. These shifts are the result of combination bands arising from the broad phosphate stretching modes exciting at similar resonances to the MOFs. New peaks also appear at 1000, 1297, and 1684 cm^{-1} in the spectra for PBS-soaked UiO-67 and all enzyme/UiO-67 composites due to phosphate stretching from adsorbed phosphate ion in the MOF pores.

The spectra of the synthesized UiO-66 (Figure 2a) and UiO-66-NH$_2$ (Figure 2b) powder products show stretching frequencies consistent with those reported in the literature.[59−61] The UiO-66-NH$_2$ shows additional broad peaks at 3500 and 3350 cm^{-1} and a moderate peak at 1650 cm^{-1} due to N-H stretching and bending that is not observed in the UiO-66 product. These major product peaks are retained in the buffer-soaked MOFs and enzyme-functionalized composites after immobilization using both MOPSO and PBS. The MOF powders soaked in PBS and the enzyme/MOF composites immobilized in PBS, however, show new peaks at 1000 and 1297 cm^{-1} similar to what is observed in UiO-67. These stretching frequencies can also be attributed to phosphate adsorbed into the pores of the MOF substrates. The intensities of these stretching frequencies, however, are much weaker compared to the characteristic product peaks for UiO-66 and UiO-66-NH$_2$. This is likely an indication of less phosphate ion adsorbed into void spaces, which is consistent with the smaller pore volume of both UiO-66 and UiO-66-NH$_2$. The spectra for UiO-67 soaked in PBS, on the other hand, shows more intense phosphate stretching that is likely a result of more phosphate ions adsorbed into the larger pore volume of the MOFs.

3.3. SEM of Enzyme/MOF Composites.
Each sample was prepared by vigorously washing in DI water after soaking in the buffer to remove free ions from the solution that were not adsorbed to the composite. The washed samples were then dried on a high vacuum line at room temperature for 12 h before being analyzed by SEM. All samples were precoated using 5 nm Au nanoparticles to reduce charging. Figure 3
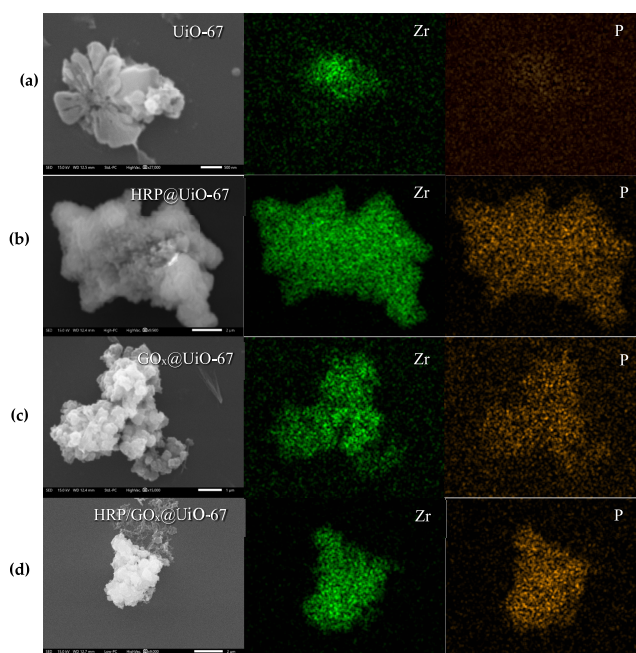

Figure 3. SEM images of MOF composites. (a) UiO-67 soaked in PBS, (b) HRP@UiO-67 immobilized in PBS, (c) GO$_x$@UiO-67 immobilized in PBS, and (d) HRP/GO$_x$@UiO-67 immobilized in PBS.

shows SEM images of UiO-67 after soaking in phosphate buffer (a), as well as the enzyme/MOF composites HRP@UiO-67 (b), GO$_x$@UiO-67 (c), and HRP/GO$_x$@UiO-67 (d) prepared using PBS during immobilization. Elemental mapping for zirconium (green) and phosphorus (gold) from EDS analysis of each substance is also shown to the right of each image. The images all show clusters of MOF particles with morphologies that exhibit irregular octahedrons characteristic of UiO-67.[28] These irregular octahedral structures are less prevalent than what would be expected for pristine UiO-67 due to the presence of adsorbed phosphate ions and phosphate salts as well as some enzyme functionalization. The elemental maps of zirconium suggest the UiO-67 framework is retained after exposure to PBS, but the elemental map of phosphorus shows phosphate has infiltrated the surface of the MOFs in the PBS-soaked UiO-67 and all enzyme/MOF composites immobilized with PBS. Additionally, these maps show the phosphate is highly dispersed throughout UiO-67 in all the enzyme/MOF composites, and not concentrated in specific regions. The presence of phosphorus in all the images analyzed strongly suggests that phosphate from the buffer is adsorbing into the MOFs and co-precipitating with the zirconium nodes as a single crystal. This co-crystallization of zirconium and phosphate demonstrated by the SEM images and elemental maps further supports the aforementioned IR and enzyme activity data.

3.4. Zeta Potential Characterization.
To further demonstrate how adsorbed phosphate ions could potentially affect enzyme loading, the zeta potentials of pure MOF and enzyme/MOF composites were measured. Zeta potential can be used to predict enzyme immobilization success by monitoring changes in electrostatic charges at the MOF surface before and after enzyme immobilization.[62,63] As shown in Table 2, all solutions of MOF and enzyme/MOF composites prepared in PB exhibited zeta potentials ranging

Table 2. Zeta Potentials of MOFs and Enzymes/MOF Composites

composite	phosphate buffer (mV)	MOPSO buffer (mV)
UiO-66	−17.6	−18.00
HRP/GO$_x$@UiO-66	−19.5	−10.80
UiO-66-NH$_2$	−18.1	−26.67
HRP/GO$_x$@UiO-66-NH$_2$	−17.4	−3.13
UiO-67	−18.6	
HRP/GO$_x$@UiO-67	−20.1	

from −17.4 to −20.1 mV. The data show no substantial differences between the pure MOF and the enzyme/MOF composites suggesting a lack of enzyme loading onto the MOF during immobilization. Effective enzyme loading is expected to produce composites with lower zeta potentials compared to pure MOF due to increased aggregation of the composite particles in the solution. Results from a previous study reporting zeta potential measurements for UiO-66, UiO-66-NH$_2$, and HRP/GO$_x$@UiO-66 prepared in MOPSO buffer, where zeta potentials significantly decreased after enzyme immobilization, are shown in Table 2 for comparison.[22,33] While the composites prepared in MOPSO exhibited strong changes in zeta potential after immobilization, the composites prepared in phosphate buffer did not. This indicates that the phosphate buffer is inhibiting enzyme loading, whereas the MOPSO buffer is facilitating enzyme loading.

3.5. XRD Results. PXRD patterns of all of the enzyme/MOF composites after immobilization using either MOPSO or PBS were compared to the patterns of the as-prepared MOFs to determine the effect of the buffering systems on the MOF structure. Figure 4 shows the overlayed PXRD patterns for (a) UiO-67, (b) UiO-66, and (c) UiO-66-NH$_2$-based composites. In addition, the three MOFs were soaked in either MOPSO or PBS buffer alone without enzyme to mimic immobilization conditions (Figure 5).

UiO-66 and UiO-66-NH$_2$ samples show similar behavior. The structures of these MOFs are unaffected by soaking alone in either MOPSO buffer or phosphate buffer under the conditions that mimic immobilization without enzyme. However, the immobilization of HRP and GO$_x$ in PBS results in a significant loss of crystallinity while immobilization of HRP and GO$_x$ using MOPSO buffer does not affect the MOF structure.

PXRD of all UiO-67 MOF and UiO-67 enzyme/MOF composite samples soaked in MOPSO or PBS shows significant loss of crystallinity compared to the as-prepared UiO-67 sample. This is likely due to the decreased stability of

UiO-67 compared with UiO-66 and UiO-66-NH$_2$. The longer biphenyl linker of UiO-67 lowers its thermal and chemical stability relative to UiO-66 making the framework more susceptible to collapse when soaked in aqueous solutions for extended periods of time. The activities of the enzyme-immobilized UiO-67 biocatalyst composites are also significantly lower than those observed for the UiO-66 and UiO-66-NH$_2$ enzyme composites, indicating these stability issues also influence enzyme loading and activity.

3.6. Surface Area Analysis. Nitrogen isotherm data, shown in Figures 6 and 7, were used to compare the effects of MOPSO buffer and PBS on the surface area and pore size of the MOFs before and after enzyme immobilization, which are summarized in Table 3. Nik et al. reported surface areas of pure UiO-66, UiO-66-NH$_2$, and UiO-67 to be 857, 826, and 1998 m^2/g, respectively.[64] Our pure MOFs had surface areas of 1261.456 m^2/g for UiO-66, 1248.978 m^2/g for UiO-66-NH$_2$, and 2120.138 m^2/g for UiO-67. The surface area measurements obtained after MOFs were soaked in MOPSO were approximately 1400 m^2/g for UiO-66, 951 m^2/g for UiO-66-NH$_2$, and 259 m^2/g for UiO-67, while the surface areas for the samples soaked in PBS were lower, at 935 m^2/g for UiO-66, 850 m^2/g for UiO-66-NH$_2$, and 15 m^2/g for UiO-67. In both cases, there is a decrease in surface area for MOPSO- and PBS-soaked MOFs, however, the PBS-soaked MOFs show a significantly greater reduction. In addition, UiO-67 shows larger reductions in surface area compared with UiO-66 and UiO-66-NH$_2$, which is due to the biphenyl scaffold being more susceptible to hydrolysis than the bdc linker in the UiO-66 MOFs. This shows that UiO-67 experiences some framework collapse after soaking in buffer solutions for 24 h, while the UiO-66 MOFs maintain more structural integrity. Regardless, the surface measurement for UiO-67 after soaking in MOPSO is still significantly higher than that obtained after soaking in PBS (259 vs 15 m^2/g).

For both buffers, there was a reduction in the surface area following enzyme immobilization in all MOFs, which is attributed to pore blockage by the enzymes. However, all the PBS-soaked samples had significantly reduced surface areas, pore volumes, and average pore size values compared to the MOPSO-soaked samples, with the exception of the average pore size values of UiO-66 and UiO-66-NH$_2$ soaked in PBS, which exhibited a respective 22.8 and 5.2% increase from UiO-66 and UiO-66-NH$_2$ soaked in MOPSO. The overall reduction in surface area, total pore volume, and average pore volume for the PBS-soaked samples compared to the MOPSO-soaked samples suggests phosphate ions are not only adsorbing into the pores of the MOFs but also contributing to a loss in
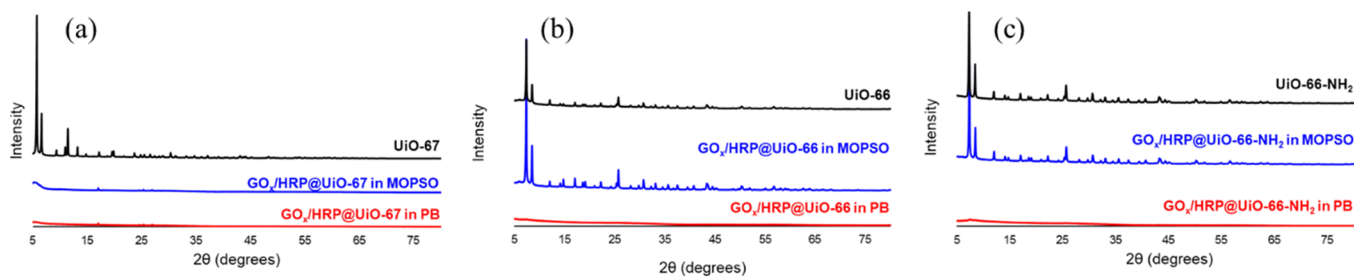

Figure 4. PXRD of MOF composites (a) as-prepared UiO-67, GO$_x$/HRP@UiO-67 immobilized in MOPSO, and GO$_x$/HRP@UiO-67 immobilized in PBS; (b) as-prepared UiO-66, GO$_x$/HRP@UiO-66 immobilized in MOPSO, and GO$_x$/HRP@UiO-66 immobilized in PBS; and (c) as-prepared UiO-66-NH$_2$, GO$_x$/HRP@UiO-66-NH$_2$ immobilized in MOPSO, and GO$_x$/HRP@UiO-66-NH$_2$ immobilized in PBS.
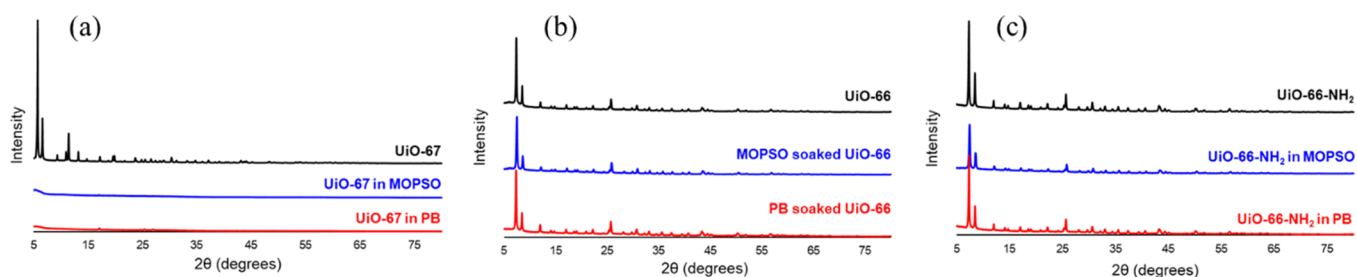
Figure 5. PXRD of MOFs (a) as-prepared UiO-67, UiO-67 soaked in MOPSO, and UiO-67 soaked in PBS; (b) as-prepared UiO-66, UiO-66 soaked in MOPSO, and UiO-66 soaked in PBS; and (c) as-prepared UiO-66-NH$_2$, UiO-66-NH$_2$ soaked in MOPSO, and UiO-66-NH$_2$ soaked in PBS.
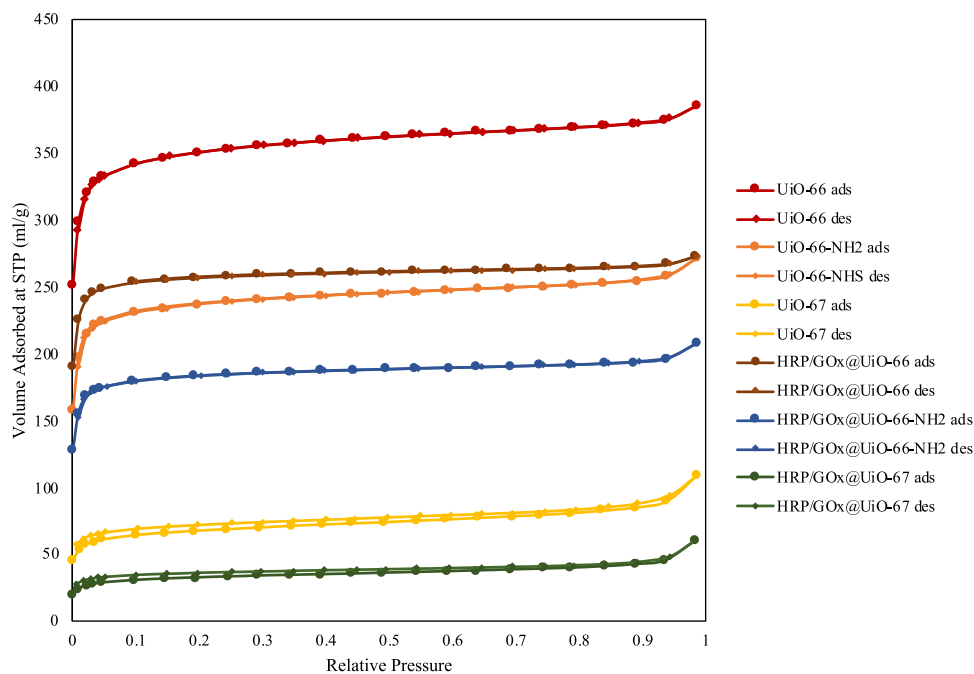

Figure 6. Adsorption−desorption curves for UiO samples after soaking in MOPSO for 24 h before drying.
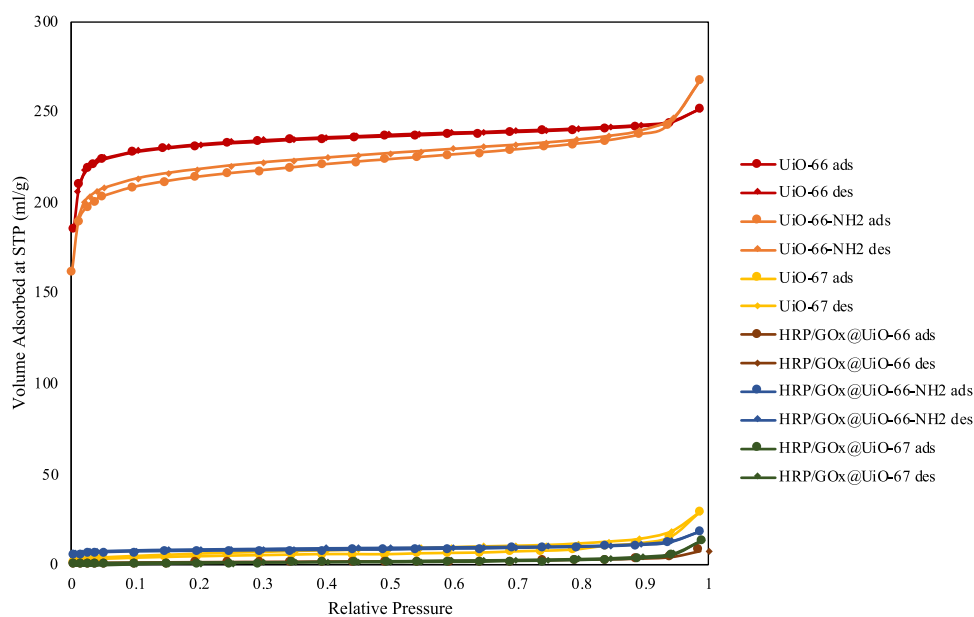

Figure 7. Adsorption−desorption curves for UiO samples after soaking in PBS for 24 h before drying.

Table 3. BET Surface Area, Total Pore Volume, and Average Pore Sizes for UiO Samples

|	sample	surface area (m^2/g)	total pore volume (mL/g)	average pore size (nm)
MOPSO	UiO-66	1399.700	0.450	9.520
	UiO-66-NH$_2$	950.955	0.296	8.883
	UiO-67	259.124	0.090	7.795
	HRP/GO$_x$@UiO-66	1044.150	0.393	11.820
	HRP/GO$_x$@UiO-66-NH2	740.45	0.2374	9.3945
	HRP/GO$_x$@UiO-67	123.952	0.0442	6.4080
phosphate buffer	UiO-66	934.666	0.320	11.597
	UiO-66-NH$_2$	849.977	0.295	9.345
	UiO-67	14.789	0.004	1.795
	HRP/GO$_x$@UiO-66	3.3509	0.0004	0.5892
	HRP/GO$_x$@UiO-66-NH2	28.1778	0.0101	5.3062
	HRP/GO$_x$@UiO-67	3.25533	−0.0024	−3.1520
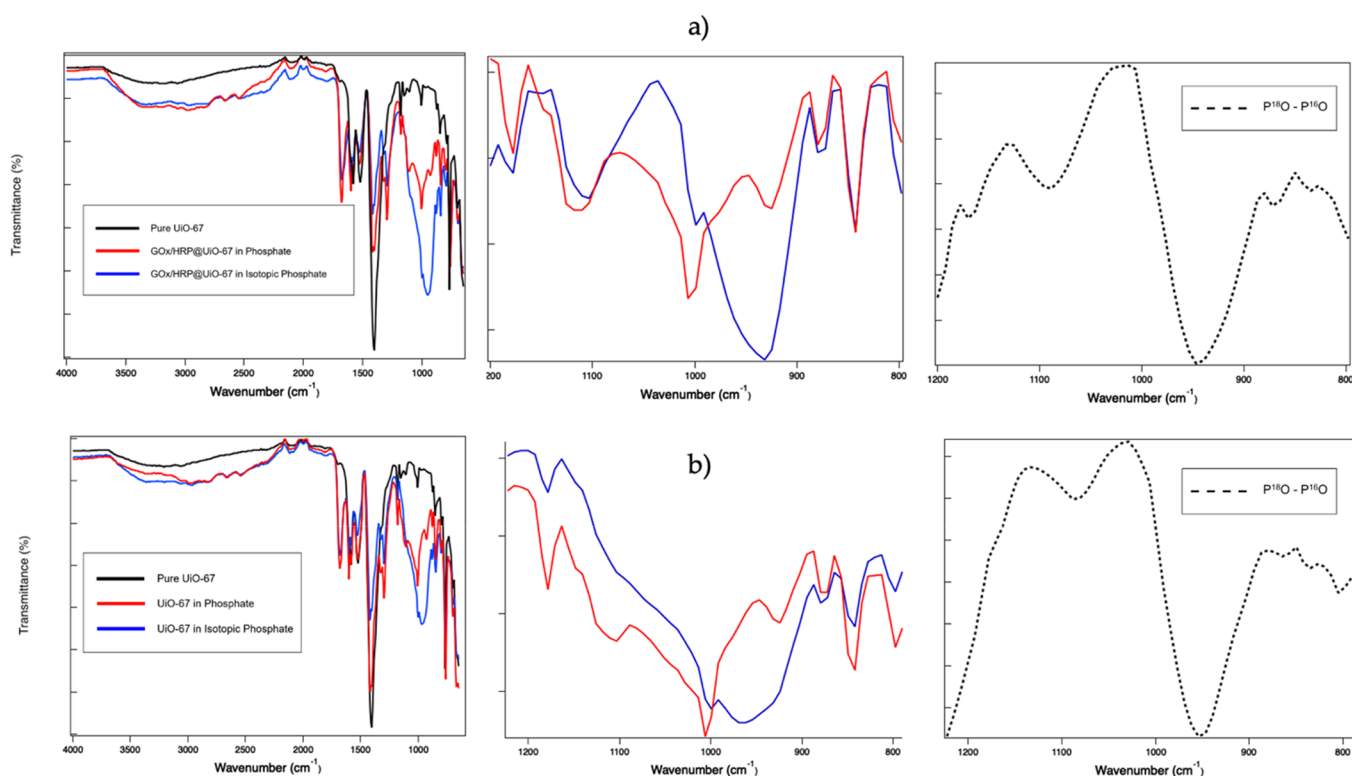
Figure 8. Isotopic shift in FT-IR spectra in phosphate buffer and isotopically labeled ^{18}O-phosphate buffer for (a) GO$_x$/HRP@UiO-67 and (b) UiO-67. Left graphs are full FT-IR spectra, middle graphs depict only the phosphate region, and the right graphs are the zoomed in difference spectra.

crystallinity during the immobilization process. Thus, the phosphate ions prevent immobilization of enzymes in phosphate-buffered systems, resulting in significantly lower surface areas and enzyme activities for all of the enzyme/MOF composites studied.

3.7. Isotopic Study. The UiO-67 MOF and the enzyme/UiO-67 composites were used in an isotope study to determine if the new resonances arising at 1000, 1297, and 1684 cm^{-1} were indeed the result of phosphate ions and not enzyme. These stretching frequencies have previously been assigned to enzyme functional groups in similar reports using MOFs for immobilization;[37,49,50,65] however, these peaks were not observed after attempting immobilization with the same enzymes using MOPSO buffer in place of PBS. Additionally, the enzyme/MOF composites immobilized in MOPSO showed superior catalytic activity compared with those immobilized in PBS. The UiO-67 MOF was chosen for this

isotopic investigation because of the larger relative intensities observed for these stretching frequencies, which were much weaker in UiO-66 and UiO-66-NH$_2$ composites.

To investigate the true origin of these stretching frequencies, an ^{18}O isotopic study of immobilization in phosphate buffer was performed to confirm if these peaks were the result of immobilized enzyme or phosphate adsorbed onto the MOF supports. The study was performed by soaking UiO-67 powder in phosphate buffer made with ^{18}O-labeled phosphate for the time required for enzyme immobilization, as well as immobilizing HRP and GO$_x$ onto UiO-67 using the same ^{18}O-labeled phosphate buffer. The resulting MOF and GO$_x$/HRP@UiO-67 composite powders that were exposed to isotopically labeled phosphate buffer were then dried and analyzed using FT-IR. The larger mass of the P—^{18}O bond created a hypsochromatic shift of the stretching frequency at

1000 cm^{-1} in the FT-IR spectra for UiO-67 and GO$_x$/HRP@ UiO-67 exposed to isotopically labeled phosphate buffer, as predicted by modeling P–O as a simple harmonic oscillator.[66,67] Using the reduced mass equation, the isotopic shift was calculated to be around 50 cm^{-1}, which is consistent with the observed shifts in the FT-IR spectra shown in Figure 8a,b of UiO-67 and immobilized GO$_x$/HRP@UiO-67 composites.

4. CONCLUSIONS

It is important to choose the appropriate microenvironment when developing new MOF/enzyme systems for effective biocatalysts. The results from this study show inhibitory effects of phosphate ion in a phosphate buffering system for co-immobilizing enzymes on UiO MOFs. A maximum decrease of 98% in enzyme's activity in phosphate immobilized composites in comparison with MOPSO buffer. The FT-IR spectra of phosphate composites showed a common peak at 1000 cm^{-1} that was confirmed to be the phosphate ion peak from an isotopic study. This result combined with the surface area, SEM, and zeta potential data confirm that phosphate ions are adsorbed by the UiO MOFs and cause partial framework collapse that adversely affects the enzyme loading and subsequently decreases catalytic activity in enzyme/UiO MOF composites immobilized using phosphate buffer. This study cautions the use of phosphate buffer in enzyme/MOF systems due to the interactions of phosphate ions with the MOFs that cause impairment in loading and activity.

■ AUTHOR INFORMATION

Corresponding Authors

Kari L. Stone − *Department of Chemistry, Lewis University, Romeoville, Illinois 60446, United States;* ◉ orcid.org/0000-0001-5942-2716; Email: kstone1@lewisu.edu

Daniel S. Kissel − *Department of Chemistry, Lewis University, Romeoville, Illinois 60446, United States;* ◉ orcid.org/0000-0003-1779-8488; Email: kisselda@lewisu.edu

Authors

Raneem Ahmad − *Department of Chemistry, Lewis University, Romeoville, Illinois 60446, United States;* Present Address: Department of Chemical Engineering, University of Michigan, Ann Arbor, Michigan 48109, United States

Sydnie Rizaldo − *Department of Chemistry, Lewis University, Romeoville, Illinois 60446, United States*

Mahnaz Gohari − *Department of Chemistry, Lewis University, Romeoville, Illinois 60446, United States*

Jordan Shanahan − *Department of Chemistry, Lewis University, Romeoville, Illinois 60446, United States;* Present Address: Department of Chemistry, University of North Carolina at Chapel Hill, Chapel Hill, North Carolina 27599, United States

Sarah E. Shaner − *Department of Chemistry and Physics, Southeast Missouri State University, Cape Girardeau, Missouri 63701, United States;* ◉ orcid.org/0000-0002-4724-6628

Complete contact information is available at:
https://pubs.acs.org/10.1021/acsomega.3c00703

Author Contributions

The manuscript was written through the contributions of all authors. All authors have given approval to the final version of the manuscript. R.A. and S.R. contributed equally.

Notes

■ REFERENCES

(1) Ren, S.; Li, C.; Jiao, X.; Jia, S.; Jiang, Y.; Bilal, M.; Cui, J. Recent Progress in Multienzymes Co-Immobilization and Multienzyme System Applications. *Chem. Eng. J.* 2019, 373, 1254−1278.

(2) Mehta, J.; Bhardwaj, N.; Bhardwaj, S. K.; Kim, K. H.; Deep, A. Recent Advances in Enzyme Immobilization Techniques: Metal-Organic Frameworks as Novel Substrates. *Coord. Chem. Rev.* 2016, 322, 30−40.

(3) Lian, X.; Fang, Y.; Joseph, E.; Wang, Q.; Li, J.; Banerjee, S.; Lollar, C.; Wang, X.; Zhou, H. C. Enzyme-MOF (Metal-Organic Framework) Composites. *Chem. Soc. Rev.* 2017, 46, 3386−3401.

(4) Sheldon, R. A.; Woodley, J. M. Role of Biocatalysis in Sustainable Chemistry. *Chem. Rev.* 2018, 118, 801−838.

(5) Homaei, A. A.; Sariri, R.; Vianello, F.; Stevanato, R. Enzyme Immobilization: An Update. *J. Chem. Biol.* 2013, 6, 185−205.

(6) Jesionowski, T.; Zdarta, J.; Krajewska, B. Enzyme Immobilization by Adsorption: A Review. *Adsorption* 2014, 20, 801−821.

(7) Mateo, C.; Palomo, J. M.; Fernandez-Lorente, G.; Guisan, J. M.; Fernandez-Lafuente, R. Improvement of Enzyme Activity, Stability and Selectivity via Immobilization Techniques. *Enzyme Microb. Technol.* 2007, 40, 1451−1463.

(8) Bosio, V. E.; Islan, G. A.; Martínez, Y. N.; Durán, N.; Castro, G. R. Nanodevices for the Immobilization of Therapeutic Enzymes. *Crit. Rev. Biotechnol.* 2016, 36, 447−464.

(9) Zare, A.; Bordbar, A. K.; Razmjou, A.; Jafarian, F. The Immobilization of Candida Rugosa Lipase on the Modified Polyethersulfone with MOF Nanoparticles as an Excellent Performance Bioreactor Membrane. *J. Biotechnol.* 2019, 289, 55−63.

(10) Cao, Y.; Wu, Z.; Wang, T.; Xiao, Y.; Huo, Q.; Liu, Y. Immobilization of: Bacillus Subtilis Lipase on a Cu-BTC Based Hierarchically Porous Metal-Organic Framework Material: A Biocatalyst for Esterification. *Dalton Trans.* 2016, 45, 6998−7003.

(11) Pisklak, T. J.; Macías, M.; Coutinho, D. H.; Huang, R. S.; Balkus, K. J. Hybrid Materials for Immobilization of MP-11 Catalyst. *Top. Catal.* 2006, 38, 269−278.

(12) Memon, A. H.; Ding, R.; Yuan, Q.; Liang, H.; Wei, Y. Coordination of GMP Ligand with Cu to Enhance the Multiple Enzymes Stability and Substrate Specificity by Co-Immobilization Process. *Biochem. Eng. J.* 2018, 136, 102−108.

(13) van Aken, B.; Ledent, P.; Naveau, H.; Agathos, S. N. Co-Immobilization of Manganese Peroxidase from Phlebia Radiata and Glucose Oxidase from Aspergillus niger on Porous Silica Beads. *Biotechnol. Lett.* 2000, 22, 641.

(14) Zare, A.; Bordbar, A. K.; Jafarian, F.; Tangestaninejad, S. Candida Rugosa Lipase Immobilization on Various Chemically Modified Chromium Terephthalate MIL-101. *J. Mol. Liq.* 2018, 254, 137−144.

(15) Betancor, L.; Luckarift, H. R. Co-Immobilized Coupled Enzyme Systems in Biotechnology. *Biotechnol. Genet. Eng. Rev.* 2010, 27, 95−114.

(16) Gustafsson, H.; Küchler, A.; Holmberg, K.; Walde, P. Co-Immobilization of Enzymes with the Help of a Dendronized Polymer

and Mesoporous Silica Nanoparticles. *J. Mater. Chem. B* **2015**, *3*, 6174−6184.

(17) Jia, F.; Narasimhan, B.; Mallapragada, S. K. Biomimetic Multienzyme Complexes Based on Nanoscale Platforms. *AIChE J.* **2013**, *59*, 355−360.

(18) Liang, K.; Ricco, R.; Doherty, C. M.; Styles, M. J.; Bell, S.; Kirby, N.; Mudie, S.; Haylock, D.; Hill, A. J.; Doonan, C. J.; et al. Biomimetic Mineralization of Metal-Organic Frameworks as Protective Coatings for Biomacromolecules. *Nat. Commun.* **2015**, *6*, 7240.

(19) Garcia-Galan, C.; Berenguer-Murcia, Á.; Fernandez-Lafuente, R.; Rodrigues, R. C. Potential of Different Enzyme Immobilization Strategies to Improve Enzyme Performance. *Adv. Synth. Catal.* **2011**, *353*, 2885−2904.

(20) Rodrigues, R. C.; Ortiz, C.; Berenguer-Murcia, Á.; Torres, R.; Fernández-Lafuente, R. Modifying Enzyme Activity and Selectivity by Immobilization. *Chem. Soc. Rev.* **2013**, *42*, 6290−6307.

(21) Bugada, L. F.; Smith, M. R.; Wen, F. Engineering Spatially Organized Multienzyme Assemblies for Complex Chemical Transformation. *ACS Catal.* **2018**, *8*, 7898−7906.

(22) Ahmad, R.; Shanahan, J.; Rizaldo, S.; Kissel, D. S.; Stone, K. L. Co-Immobilization of an Enzyme System on a Metal-Organic Framework to Produce a More Effective Biocatalyst. *Catalysts* **2020**, *10*, 499.

(23) Zhu, L.; Yang, R.; Zhai, J.; Tian, C. Bienzymatic Glucose Biosensor Based on Co-Immobilization of Peroxidase and Glucose Oxidase on a Carbon Nanotubes Electrode. *Biosens. Bioelectron.* **2007**, *23*, 528−535.

(24) Pitzalis, F.; Monduzzi, M.; Salis, A. A Bienzymatic Biocatalyst Constituted by Glucose Oxidase and Horseradish Peroxidase Immobilized on Ordered Mesoporous Silica. *Microporous Mesoporous Mater.* **2017**, *241*, 145−154.

(25) Ahmad, R.; Rizaldo, S.; Shaner, S. E.; Kissel, D. S.; Stone, K. L. Immobilization of a Bienzymatic System via Crosslinking to a Metal-Organic Framework. *Catalysts* **2022**, *12*, 969.

(26) Bankar, S. B.; Bule, M. V.; Singhal, R. S.; Ananthanarayan. Glucose Oxidase - An Overview. *Biotechnol. Adv.* **2009**, *27*, 489−501.

(27) Veitch, N. C. Horseradish Peroxidase: A Modern View of a Classic Enzyme. *Phytochemistry* **2004**, *65*, 249−259.

(28) Hashemifard, N.; Mohsenifar, A.; Ranjbar, B.; Allameh, A.; Lotfi, A. S.; Etemadikia, B. Fabrication and Kinetic Studies of a Novel Silver Nanoparticles-Glucose Oxidase Bioconjugate. *Anal. Chim. Acta* **2010**, *675*, 181−184.

(29) Ohtsu, T.; Shigenari, S.; Yoshimoto, M.; Umakoshi, H. Reactive Bienzyme Systems Fabricated through Immobilization of Biotinylated Glucose Oxidase and Peroxidase Molecules onto Neutralized Avidin-Conjugated Liposomes. *Biochem. Eng. J.* **2017**, *125*, 81−87.

(30) Betancor, L.; Fuentes, M.; Dellamora-Ortiz, G.; López-Gallego, F.; Hidalgo, A.; Alonso-Morales, N.; Mateo, C.; Guisán, J. M.; Fernández-Lafuente, R. Dextran Aldehyde Coating of Glucose Oxidase Immobilized on Magnetic Nanoparticles Prevents Its Inactivation by Gas Bubbles. *J. Mol. Catal. B: Enzym.* **2005**, *32*, 97−101.

(31) Kumar, A.; Malhotra, R.; Malhotra, B. D.; Grover, S. K. Co-Immobilization of Cholesterol Oxidase and Horseradish Peroxidase in a Sol-Gel Film. *Anal. Chim. Acta* **2000**, *414*, 43.

(32) Batten, S. R.; Champness, N. R.; Chen, X. M.; Garcia-Martinez, J.; Kitagawa, S.; Öhrström, L.; O'Keeffe, M.; Suh, M. P.; Reedijk, J. Terminology of Metal-Organic Frameworks and Coordination Polymers (IUPAC Recommendations 2013). *Pure Appl. Chem.* **2013**, *85*, 1715−1724.

(33) Shearer, G. C.; Chavan, S.; Ethiraj, J.; Vitillo, J. G.; Svelle, S.; Olsbye, U.; Lamberti, C.; Bordiga, S.; Lillerud, K. P. Tuned to Perfection: Ironing out the Defects in Metal-Organic Framework UiO-66. *Chem. Mater.* **2014**, *26*, 4068−4071.

(34) Hu, Y.; Dai, L.; Liu, D.; Du, W.; Wang, Y. Progress & Prospect of Metal-Organic Frameworks (MOFs) for Enzyme Immobilization (Enzyme/MOFs). *Renew. Sustainable Energy Rev.* **2018**, *91*, 793−801.

(35) Qin, F. X.; Jia, S. Y.; Wang, F. F.; Wu, S. H.; Song, J.; Liu, Y. Hemin@metal-Organic Framework with Peroxidase-like Activity and

Its Application to Glucose Detection. *Catal. Sci. Technol.* **2013**, *3*, 2761−2768.

(36) Dhaka, S.; Kumar, R.; Deep, A.; Kurade, M. B.; Ji, S. W.; Jeon, B. H. Metal−Organic Frameworks (MOFs) for the Removal of Emerging Contaminants from Aquatic Environments. *Coord. Chem. Rev.* **2019**, *380*, 330−352.

(37) Liu, W. L.; Yang, N. S.; Chen, Y. T.; Lirio, S.; Wu, C. Y.; Lin, C. H.; Huang, H. Y. Lipase-Supported Metal-Organic Framework Bioreactor Catalyzes Warfarin Synthesis. *Chem. − Eur. J.* **2015**, *21*, 115−119.

(38) Shih, Y. H.; Lo, S. H.; Yang, N. S.; Singco, B.; Cheng, Y. J.; Wu, C. Y.; Chang, I. H.; Huang, H. Y.; Lin, C. H. Trypsin-Immobilized Metal-Organic Framework as a Biocatalyst in Proteomics Analysis. *Chempluschem* **2012**, *77*, 982−986.

(39) Wang, X.; Lu, X.; Wu, L.; Chen, J. 3D Metal-Organic Framework as Highly Efficient Biosensing Platform for Ultrasensitive and Rapid Detection of Bisphenol A. *Biosens. Bioelectron.* **2015**, *65*, 295−301.

(40) Gkaniatsou, E.; Sicard, C.; Ricoux, R.; Mahy, J. P.; Steunou, N.; Serre, C. Metal-Organic Frameworks: A Novel Host Platform for Enzymatic Catalysis and Detection. *Mater. Horiz.* **2017**, *4*, 55−63.

(41) Jung, S.; Kim, Y.; Kim, S. J.; Kwon, T. H.; Huh, S.; Park, S. Bio-Functionalization of Metal-Organic Frameworks by Covalent Protein Conjugation. *Chem. Commun.* **2011**, *47*, 2904−2906.

(42) Wu, X.; Yang, C.; Ge, J. Green Synthesis of Enzyme/Metal-Organic Framework Composites with High Stability in Protein Denaturing Solvents. *Bioresour. Bioprocess.* **2017**, *4*, 24.

(43) Feng, D.; Liu, T. F.; Su, J.; Bosch, M.; Wei, Z.; Wan, W.; Yuan, D.; Chen, Y. P.; Wang, X.; Wang, K.; et al. Stable Metal-Organic Frameworks Containing Single-Molecule Traps for Enzyme Encapsulation. *Nat. Commun.* **2015**, *6*, 5979.

(44) Raja, D. S.; Liu, W. L.; Huang, H. Y.; Lin, C. H. Immobilization of Protein on Nanoporous Metal-Organic Framework Materials. *Comments Inorg. Chem.* **2015**, *35*, 331−349.

(45) Abid, H. R.; Shang, J.; Ang, H. M.; Wang, S. Amino-Functionalized Zr-MOF Nanoparticles for Adsorption of CO_2 and CH_4. *Int. J. Smart Nano Mater.* **2013**, *4*, 72−82.

(46) Cao, S. L.; Yue, D. M.; Li, X. H.; Smith, T. J.; Li, N.; Zong, M. H.; Wu, H.; Ma, Y. Z.; Lou, W. Y. Novel Nano−/Micro-Biocatalyst: Soybean Epoxide Hydrolase Immobilized on UiO-66-NH2 MOF for Efficient Biosynthesis of Enantiopure (R)-1, 2-Octanediol in Deep Eutectic Solvents. *ACS Sustainable Chem. Eng.* **2016**, *4*, 3586−3595.

(47) Huo, J.; Aguilera-Sigalat, J.; El-Hankari, S.; Bradshaw, D. Magnetic MOF Microreactors for Recyclable Size-Selective Biocatalysis. *Chem. Sci.* **2015**, *6*, 1938−1943.

(48) Patra, S.; Hidalgo Crespo, T.; Permyakova, A.; Sicard, C.; Serre, C.; Chaussé, A.; Steunou, N.; Legrand, L. Design of Metal Organic Framework-Enzyme Based Bioelectrodes as a Novel and Highly Sensitive Biosensing Platform. *J. Mater. Chem. B* **2015**, *3*, 8983−8992.

(49) Wang, J.; Zhao, G.; Yu, F. Facile Preparation of Fe3O4@MOF Core-Shell Microspheres for Lipase Immobilization. *J. Taiwan Inst. Chem. Eng.* **2016**, *69*, 139−145.

(50) Samui, A.; Chowdhuri, A. R.; Mahto, T. K.; Sahu, S. K. Fabrication of a Magnetic Nanoparticle Embedded NH2-MIL-88B MOF Hybrid for Highly Efficient Covalent Immobilization of Lipase. *RSC Adv.* **2016**, *6*, 66385−66393.

(51) Taha, M.; Lee, M. J. Solubility and Phase Separation of 4-Morpholinepropanesulfonic Acid (MOPS), and 3-Morpholino-2-Hydroxypropanesulfonic Acid (MOPSO) in Aqueous 1,4-Dioxane and Ethanol Solutions. *J. Chem. Thermodyn.* **2011**, *43*, 1723−1730.

(52) Ramasarma, T.; Rao, A. V. S.; Devi, M. M.; Omkumar, R.; Bhagyashree, K. S.; Bhat, S. V. New Insights of Superoxide Dismutase Inhibition of Pyrogallol Autoxidation. *Mol. Cell. Biochem.* **2015**, *400*, 277−285.

(53) Critchlow, A.; Haslam, E.; Haworth, R. D.; Tinker, P. B.; Waldron, N. M. The Oxidation Of Some Pyrogallol And Purpurogallin Derivatives. *Tetrahedron* **1967**, *23*, 2829.

(54) Kornecki, J. F.; Carballares, D.; Morellon-Sterling, R.; Siar, E. H.; Kashefi, S.; Chafiaa, M.; Arana-Peña, S.; Rios, N. S.; Gonçalves, L.

R. B.; Fernandez-Lafuente, R. Influence of Phosphate Anions on the Stability of Immobilized Enzymes. Effect of Enzyme Nature, Immobilization Protocol and Inactivation Conditions. *Process Biochem.* **2020**, *95*, 288−296.

(55) Velásquez-Hernández, M. D. J.; Ricco, R.; Carraro, F.; Limpoco, F. T.; Linares-Moreau, M.; Leitner, E.; Wiltsche, H.; Rattenberger, J.; Schröttner, H.; Frühwirt, P.; et al. Degradation of ZIF-8 in Phosphate Buffered Saline Media. *CrystEngComm* **2019**, *21*, 4538−4544.

(56) Zaak, H.; Fernandez-Lopez, L.; Velasco-Lozano, S.; Alcaraz-Fructuoso, M. T.; Sassi, M.; Lopez-Gallego, F.; Fernandez-Lafuente, R. Effect of High Salt Concentrations on the Stability of Immobilized Lipases: Dramatic Deleterious Effects of Phosphate Anions. *Process Biochem.* **2017**, *62*, 128−134.

(57) Agostoni, V.; Chalati, T.; Horcajada, P.; Willaime, H.; Anand, R.; Semiramoth, N.; Baati, T.; Hall, S.; Maurin, G.; Chacun, H.; Bouchemal, K.; Martineau, C.; Taulelle, F.; Couvreur, P.; Rogez-Kreuz, C.; Clayette, P.; Monti, S.; Serre, C.; Gref, R. Towards an Improved Anti-HIV Activity of NRTI via Metal-Organic Frameworks Nanoparticles. *Adv. Healthcare Mater.* **2013**, *2*, 1630−1637.

(58) Fernandez, M.; Frydman, R. B.; Hurst, J.; Buldain, G. Structure/Activity Relationships in Porphobilinogen Oxygenase and Horseradish Peroxidase: An Analysis Using Synthetic Hemins. *Eur. J. Biochem.* **1993**, *218*, 251−259.

(59) Cavka, J. H.; Jakobsen, S.; Olsbye, U.; Guillou, N.; Lamberti, C.; Bordiga, S.; Lillerud, K. P. A New Zirconium Inorganic Building Brick Forming Metal Organic Frameworks with Exceptional Stability. *J. Am. Chem. Soc.* **2008**, *130*, 13850−13851.

(60) Valenzano, L.; Civalleri, B.; Chavan, S.; Bordiga, S.; Nilsen, M. H.; Jakobsen, S.; Lillerud, K. P.; Lamberti, C. Disclosing the Complex Structure of UiO-66 Metal Organic Framework: A Synergic Combination of Experiment and Theory. *Chem. Mater.* **2011**, *23*, 1700−1718.

(61) Kandiah, M.; Nilsen, M. H.; Usseglio, S.; Jakobsen, S.; Olsbye, U.; Tilset, M.; Larabi, C.; Quadrelli, E. A.; Bonino, F.; Lillerud, K. P. Synthesis and Stability of Tagged UiO-66 Zr-MOFs. *Chem. Mater.* **2010**, *22*, 6632−6640.

(62) Ma, W.; Jiang, Q.; Yu, P.; Yang, L.; Mao, L. Zeolitic Imidazolate Framework-Based Electrochemical Biosensor for in Vivo Electrochemical Measurements. *Anal. Chem.* **2013**, *85*, 7550−7557.

(63) Schultz, N.; Metreveli, G.; Franzreb, M.; Frimmel, F. H.; Syldatk, C. Zeta Potential Measurement as a Diagnostic Tool in Enzyme Immobilisation. *Colloids Surf., B* **2008**, *66*, 39−44.

(64) Nik, O. G.; Chen, X. Y.; Kaliaguine, S. Functionalized metal organic framework-polyimide mixed matrix membranes for CO2/CH4 separation. *J. Membr. Sci.* **2012**, *416-414*, 48−61.

(65) Hu, S.; Hager, L. P. Unusual Propargylic Oxidations Catalyzed by Chloroperoxidase. *Biochem. Biophys. Res. Commun.* **1998**, *253*, 544.

(66) Valentin, R.; Bonelli, B.; Garrone, E.; di Renzo, F.; Quidnard, F. Accessibility of the Functional Group of Chitosan Aerogel Probed by FT-IR-Monitored Deuteration. *Biomacromolecules* **2007**, *8*, 3646−3650.

(67) Cushing, J. T. Relativistic Bohr Model with Finite-Mass Nucleus. *Am. J. Phys.* **1970**, *38*, 1145−1150.